

# Monte Carlo simulations of the disk white dwarf population

Enrique García-Berro<sup>1</sup>, Santiago Torres<sup>2</sup>, Jordi Isern<sup>3</sup>, and Andreas Burkert<sup>4</sup>

<sup>1</sup>*Departament de Física Aplicada, Universitat Politècnica de Catalunya & Institut d'Estudis Espacials de Catalunya/UPC, Jordi Girona Salgado s/n, Mòdul B-4, Campus Nord, 08034 Barcelona, Spain*

<sup>2</sup>*Departament de Telecomunicació i Arquitectura de Computadors, E.U.P. de Mataró, Universitat Politècnica de Catalunya, Av. Puig i Cadafalch 101, 08303 Mataró, Spain*

<sup>3</sup>*Institut d'Estudis Espacials de Catalunya/C.S.I.C., Edifici Nexus, Gran Capità 2-4, 08034 Barcelona, Spain*

<sup>4</sup>*Max-Planck-Institut für Astronomie, Königstuhl 17, 69117 Heidelberg, Germany*

29 September 2018

## ABSTRACT

In order to understand the dynamical and chemical evolution of our Galaxy it is of fundamental importance to study the local neighborhood. White dwarf stars are ideal candidates to probe the history of the solar neighborhood, since these “fossil” stars have very long evolutionary time-scales and, at the same time, their evolution is relatively well understood. In fact, the white dwarf luminosity function has been used for this purpose by several authors. However, a long standing problem arises from the relatively poor statistics of the samples, especially at low luminosities. In this paper we assess the statistical reliability of the white dwarf luminosity function by using a Monte Carlo approach.

**Key words:** stars: white dwarfs — stars: luminosity function, mass function — Galaxy: stellar content

## 1 INTRODUCTION

The white dwarf luminosity function has become an important tool to determine some properties of the local neighborhood, such as its age (Winget et al. 1987; García-Berro et al. 1988; Hernanz et al. 1994), or the past history of the star formation rate (Noh & Scalo 1990; Díaz-Pinto et al. 1994; Isern et al. 1995a,b). This has been possible because now we have improved observational luminosity functions (Liebert, Dahn & Monet 1988; Oswalt et al. 1996; Leggett, Ruiz & Bergeron 1998) and because we have a better understanding of the physics of white dwarfs and, consequently, reliable cooling sequences — at least up to moderately low luminosities.

The most important features of the luminosity function of white dwarfs are a smooth increase up to luminosities of  $\log(L/L_{\odot}) \sim -4.0$ , and the presence of a pronounced cut-off at  $\log(L/L_{\odot}) \sim -4.4$ , although its exact position is still today somehow uncertain since it hinges on the statistical significance of a small subset of objects, on how the available data is binned and on the fine details of the sampling procedure. Most of the information on the early times of the past history of the local neighborhood is concentrated on this uncertain low luminosity portion of the white dwarf luminosity function.

A major drawback of the luminosity function of white

dwarfs is that it measures the volumetric density of white dwarfs and, therefore, in order to compare with the observations one must use the volumetric star formation rate, that is the star formation rate per cubic parsec, whereas for many studies of galactic evolution the star formation rate per square parsec is required and, consequently, fitted to the observations.

Another important issue is the fact that the sample from which the low luminosity portion ( $M_V > 13^{\text{mag}}$ ) of the white dwarf luminosity function is derived has been selected on a kinematical basis (white dwarfs with relatively high proper motions). Therefore, some kinematical biases or distortions are expected. Although there are some studies of the kinematical properties of white dwarf stars — see, for instance, Sion et al. (1988) and references therein — a complete and comprehensive kinematical study of the sample used to obtain the white dwarf luminosity function remains to be done. It is important to realize that a conventional approach to compute theoretical luminosity functions (Hernanz et al. 1994; Wood 1992) does not take into account the kinematical properties of the observed sample. A Monte Carlo simulation of a model population of white dwarfs is expected to allow the biases and effects of sample selection to be taken into account, so their luminosity function could be corrected — or, at least, correctly interpreted — provided

that a detailed simulation from the stage of source selection is performed accurately. Of course, a realistic model of the evolution of our Galaxy is required for that purpose.

Finally, the available white dwarf luminosity functions (Liebert et al. 1988; Oswalt et al. 1996, Leggett et al. 1988) have been obtained using the  $1/V_{\max}$  method (Schmidt 1968), which assumes a uniform distribution of the objects, yet nothing in our local neighborhood is, strictly speaking, homogeneous. In fact, stars in the solar neighborhood are concentrated in the plane of the galactic disk. Moreover, it is expected that old objects should have larger scale heights than young ones. This dependence on the scale height probably has effects on the observed white dwarf luminosity function — especially on its low luminosity portion where old objects concentrate — and, once again, a realistic model of galactic evolution is required for evaluating the effects of the departures from homogeneity of the observed samples. To our knowledge, this effect was only taken into account for the bright portion of the white dwarf luminosity function (Fleming, Liebert & Green 1986) and not for the low luminosity portion where the effects are expected to be more dramatic.

Perhaps the most successful application of the white dwarf luminosity function has been its invaluable contribution as an independent galactic chronometer to a better understanding of our Galaxy. Despite this fact there have been very few attempts — being those of García-Berro & Torres (1997), Wood (1997) and Wood & Oswalt (1998) the only serious ones — to systematically investigate the statistical uncertainties associated with the derived age of the disk. Nevertheless the approach used by Wood & Oswalt (1998) makes use of the *observed* kinematic properties of the white dwarf population instead of using a standard model of the evolution of our Galaxy, which presumably should include the effects of a scale height law. Besides, these authors use the theoretical white dwarf luminosity function obtained from standard methods to assign probabilities and, ultimately, to assign luminosities to the white dwarfs of the sample. Finally, in their calculations Wood & Oswalt (1998) computed the cooling times of all the white dwarfs of their sample by interpolating in a model cooling sequence of a  $0.6 M_{\odot}$  white dwarf, thus neglecting the effects of the full mass spectrum of white dwarfs.

In this paper we explore the statistical reliability and completeness of the white dwarf luminosity function taking into account all of the above mentioned effects that were disregarded in previous studies. Special emphasis will be placed on the statistical significance of the reported cut-off in the white dwarf luminosity function. For that purpose we will use a Monte Carlo method, coupled with bayesian inference techniques, within the frame of a consistent model of galactic evolution, and using improved cooling sequences.

To be precise, we want specific answers for the following questions: are the kinematics of the derived white dwarf population consistent with the observational data? Which are the effects of a scale height in the observed samples? Is the sample used to derive the white dwarf luminosity function representative of the whole white dwarf population? Or, at least, is this sample compatible with the white dwarf population within the limits imposed by the selection procedure? Which are the statistical errors for each luminosity

bin? Which is the typical sampling error in the derived age of the disk?

The paper is organized as follows: in §2 we describe how the simulated population of white dwarfs is built; in §3 we describe the kinematical properties of the samples obtained in this way and we compare them with those of a real, although very preliminary and possibly uncomplete, sample; in §4 we study the spatial distribution of the samples, we assess the statistical reliability and completeness of the white dwarf luminosity function and we derive an estimate of the error budget in the determination of the age of the disk; finally, in §5 our results are summarized, followed by conclusions and suggestions for future improvements.

## 2 BUILDING THE SAMPLE

The basic ingredient of any Monte Carlo code is a generator of random variables distributed according to a given probability density. The simulations described in this paper have been done using a random number generator algorithm (James 1990) which provides a uniform probability density within the interval  $(0, 1)$  and ensures a repetition period of  $\gtrsim 10^{18}$ , which is virtually infinite for practical simulations. When gaussian probability functions are needed we have used the Box-Muller algorithm as described in Press et al. (1986).

We randomly choose two numbers for the galactocentric polar coordinates  $(r, \theta)$  of each star in the sample within approximately 200 pc from the sun, assuming a constant surface density. The density changes due to the radial scale length of our Galaxy are negligible over the distances we are going to consider here and can be completely ignored. Next we draw two more pseudo-random numbers: the first for the mass ( $M$ ) on the main sequence of each star — according to the initial mass function of Scalo (1998) — and the second for the time at which each star was born ( $t_b$ ) — according to a given star formation rate. We have chosen an exponentially decreasing star formation rate per unit time and unit surface:  $\psi \propto e^{-t/\tau_s}$ . This choice of the shape of the star formation rate is fully consistent with our current understanding of the chemical evolution of our Galaxy — see, for instance, Bravo et al. (1993). Once we know the time at which each star was born we assign the  $z$  coordinate by drawing another random number according to an exponential disk profile. The scale height of newly formed stars adopted here decreases exponentially with time:  $H_p(t) = z_i e^{-t/\tau_h} + z_f$ . This choice for the time dependence of the scale height is essentially arbitrary, although it can be considered natural. We will however show that using these prescriptions for both the surface star formation rate and the scale height law to compute the theoretical white dwarf luminosity function leads to an excellent fit to the observations (see Isern et al. 1995a,b and §4) which does not result in a conflict with the observed kinematics of the white dwarf population (see §3). The values of the free parameters for both the surface star formation rate and the scale height have been taken from Isern et al. (1995a,b), namely:  $\tau_s = 24$  Gyr,  $\tau_h = 0.7$  Gyr,  $z_i/z_f = 485$ .

In order to determine the heliocentric velocities in the  $B3$  system,  $(U, V, W)$ , of each star in the sample three more

quantities are drawn according to normal laws:

$$\begin{aligned} n(U) &\propto e^{-(U-U'_0)^2/\sigma_U^2} \\ n(V) &\propto e^{-(V-V'_0)^2/\sigma_V^2} \\ n(W) &\propto e^{-(W-W'_0)^2/\sigma_W^2} \end{aligned} \quad (1)$$

where  $(U'_0, V'_0, W'_0)$  take into account the differential rotation of the disk (Ogorodnikov 1965), and derive from the peculiar velocity  $(U_\odot, V_\odot, W_\odot)$  of the sun for which we have adopted the value  $(10, 5, 7)$  km s<sup>-1</sup> (Dehnen & Binney 1997).

The three velocity dispersions  $(\sigma_U, \sigma_V, \sigma_W)$ , and the lag velocity,  $V_0$ , of a given sample of stars are not independent of the scale height. From main sequence star counts, Mihalas & Binney (1981) obtain the following relations, when the velocities are expressed in km s<sup>-1</sup> and the scale height is expressed in kpc:

$$\begin{aligned} U_0 &= 0 \\ V_0 &= -\sigma_U^2/120 \\ W_0 &= 0 \end{aligned} \quad (2)$$

$$\begin{aligned} \sigma_V^2/\sigma_U^2 &= 0.32 + 1.67 \cdot 10^{-5} \sigma_U^2 \\ \sigma_W^2/\sigma_U^2 &= 0.50 \\ H_p &= 6.52 \cdot 10^{-4} \sigma_U^2 \end{aligned}$$

which is what we adopt here (see as well §3.3). Note, however, that our most important input is the scale height law, from which most of the kinematical quantities are derived.

Since white dwarfs are long lived objects the effects of the galactic potential on their motion, and therefore on their positions and proper motions, can be potentially large, especially for very old objects which populate the tail of the white dwarf luminosity function. Therefore, the  $z$  coordinate is integrated using the galactic potential proposed by Flynn et al. (1996). This galactic potential includes the contributions of the disk, the bulge and the halo, and reproduces very well the local disk surface density of matter and the rotation curve of our Galaxy. We do not consider the effects of the galactic potential in the  $r$  and  $\theta$  coordinates. This is the same as assuming that the number of white dwarfs that enter into the sector of the disk that we are considering (the local column) is, on average, equal to the number of white dwarfs that are leaving it. Of course, with this approach we are neglecting the possibility of a global radial flow, and thus, the possible effects of diffusion across the disk. However, the observed disk kinematics suggest that radial mixing is efficient up to distances much larger than the maximum distance we have used in our simulations (Carney, Latham & Laird 1990).

From this set of data we can now compute parallaxes and proper motions for all the stars ( $\sim 200\,000$ ) in the sample. Given the age of the disk ( $t_{\text{disk}}$ ) we can also compute how many of these stars have had time to evolve to white dwarfs and, given a set of cooling sequences (Salaris et al. 1997, García-Berro et al. 1997), what are their luminosities. This set of cooling sequences includes the effects of phase separation of carbon and oxygen upon crystallization and has been computed taking into account detailed chemical profiles of the carbon-oxygen binary mixture present in most white dwarf interiors. These chemical profiles have been obtained using the most up to date treatment of the effects

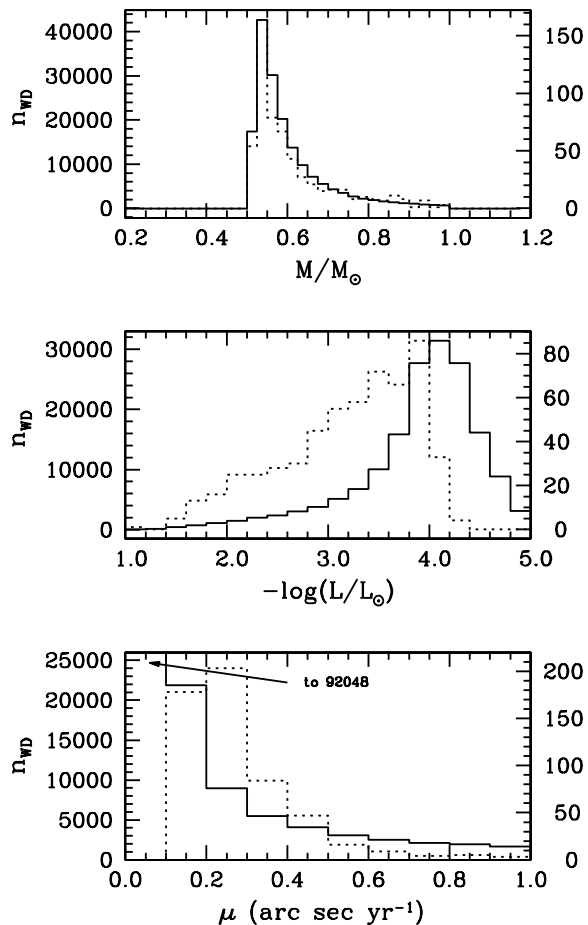


**Figure 1.** Some relevant distributions obtained from a single Monte Carlo simulation, the solid lines correspond to the original sample whereas the dotted lines correspond to the restricted sample. See text for details.

of an enhanced reaction rate for the  $^{12}\text{C}(\alpha, \gamma)^{16}\text{O}$  reaction. Of course, a relationship between the mass on the main sequence and the mass of the resulting white dwarf is needed. Main sequence lifetimes must be provided as well. For these two relationships we have used those of Iben & Laughlin (1989). The size of this new sample of white dwarfs typically is of  $\sim 60\,000$  stars (hereinafter “original” sample). Finally, for all white dwarfs belonging to this sample bolometric corrections are calculated by interpolating in the atmospheric tables of Bergeron et al. (1995) and their  $V$  magnitude is obtained, assuming that all are non-DA white dwarfs.

Since the final goal is to compute the white dwarf luminosity function using the  $1/V_{\text{max}}$  method (Schmidt 1968) a set of restrictions is needed for selecting a subset of white dwarfs which, in principle, should be representative of the whole white dwarf population. We have chosen the following criteria for selecting the final sample:  $m_V \leq 18.5^{\text{mag}}$  and  $\mu \geq 0.16'' \text{ yr}^{-1}$  (Oswalt et al. 1996). We do not consider white dwarfs with very small parallaxes ( $\pi \leq 0.005''$ ), since these are unlikely to belong to a realistic observational sample. All white dwarfs brighter than  $M_V \leq 13^{\text{mag}}$  are included in the sample, regardless of their proper motions, since the the luminosity function of hot white dwarfs has been obtained from a catalog of spectroscopically identified white dwarfs (Green 1980; Fleming et al. 1986) which is assumed

to be complete. Additionally all white dwarfs with tangential velocities larger than  $250 \text{ km s}^{-1}$  were discarded (Liebert, Dahn & Monet 1989) since these would be probably classified as halo members. These restrictions determine the size of the the final sample which typically is  $\sim 200$  stars (hereinafter “restricted” sample). Finally we normalize the total density of white dwarfs obtained in this way to its observed value in the solar neighborhood (Oswalt et al. 1996).

In Figure 1 we show a summary of the most relevant results for a disk age of 13 Gyr. In the top panel, the mass distribution of those stars that have been able to become white dwarfs (solid line, left scale) and of those white dwarfs that are selected for computing the luminosity function (dotted line, right scale) are shown. Both distributions are well behaved, follow closely each other, and peak at around  $0.55 M_{\odot}$  in very good agreement with the observations (Bergeron, Saffer & Liebert 1992). In this sense, the restricted sample could be considered as representative of the whole white dwarf population.

In the middle panel of figure 1 we show the raw distribution of luminosities for the stars in the original (solid line, left scale) and the restricted (dotted line, right scale) samples. The differences between both distributions are quite apparent: first, the restricted sample has a broad peak centered at  $\log(L/L_{\odot}) \sim -3.5$ , whereas the original sample is narrowly peaked at a smaller luminosity (0.6 dex). Obviously, since the restricted sample is selected on a kinematical basis — see the lower panel of figure 1, where the distribution of proper motions for both samples is shown — some very faint and low proper motion white dwarfs are discarded. Thus, the restricted sample is biased towards larger luminosities. Therefore, the cut-off of the observational luminosity function should be biased as well towards larger luminosities. However, it is important to realize that only  $\sim 0.6\%$  of the total number of white dwarfs with  $\log(L/L_{\odot}) > -4.0$  are selected for the restricted sample, and therefore, used in computing the white dwarf luminosity function. This number decreases to  $\sim 0.04\%$  if we consider the low luminosity portion of the white dwarf luminosity function — that is, white dwarfs with  $\log(L/L_{\odot}) < -4.0$  — where most of the information regarding the initial phases of our Galaxy is recorded. The distribution of proper motions (lower right panel of figure 1) shows that most white dwarfs for both the original and the restricted sample have proper motions smaller than  $0.4'' \text{ yr}^{-1}$ . However, the restricted sample has a pronounced peak at  $\mu \sim 0.3'' \text{ yr}^{-1}$ , and shows a deficit of very low proper motion white dwarfs, as should be the case for a kinematically selected sample, whereas the original sample smoothly decreases for increasing proper motions.

### 3 THE KINEMATIC PROPERTIES OF THE WHITE DWARF POPULATION

Since the pioneering work of Sion & Liebert (1977), very few analysis of the kinematics of the white dwarf population have been done, with that of Sion et al. (1988) being the most relevant one, despite the fact that the low luminosity portion of the white dwarf luminosity function is actually derived from a kinematically selected sample. Sion et al. (1988) used a specific subset of the proper-motion sample of spectroscopically identified white dwarfs to check kinematically

distinct spectroscopic subgroups and test different scenarios of white dwarf production channels. However, a major disadvantage of this subset of the white dwarf population is that the three components of the velocity are derived only from the tangential velocity, since the determination of radial velocities for white dwarfs is not an easy task, especially for very cool ones. Obviously it would be better to have the complete description of the space motions of this sample, but it is nonetheless true that we already have two-thirds of the motion available for comparison with the simulated samples and that the latter samples can account for this observational bias.

The sample of Sion et al. (1988) consists of 626 stars with known distances and tangential velocities (of which 421 white dwarfs belong to the spectral type DA and 205 stars belong to other spectral types). In this proper motion sample there are 523 white dwarfs for which masses, radii and effective temperatures could be derived — see Sion et al. (1988) for the computational details — of which 372 have masses larger than  $0.5 M_{\odot}$  and, therefore, are expected to have carbon-oxygen cores. Of this latter group of white dwarfs there are 305 with spectral type DA and 67 belong to other spectral types. For this particular sample of white dwarfs cooling ages were derived using the cooling sequences of Salaris et al. (1997) and, given a relationship between the initial mass on the main sequence and the final mass of the white dwarf (Iben & Laughlin 1989), main sequence lifetimes (Iben & Laughlin 1989) were also assigned, and the birth time of their progenitors was computed. However, the errors in the determination of the mass of the progenitor can produce large errors in the determination of the total age of low mass white dwarfs. For instance, for a typical  $0.6 M_{\odot}$  white dwarf an error in the determination of its mass of  $0.05 M_{\odot}$  leads to an error in its cooling age of  $\sim 0.3$  Gyr at  $\log(L/L_{\odot}) = -2.0$  and of  $\sim 0.8$  Gyr at  $\log(L/L_{\odot}) = -4.0$ , whereas the error in the determination of its main sequence lifetime is of  $\sim 2$  Gyr. Thus, the mass dependence of the cooling sequences is relatively small, whereas the mass dependence of the main sequence lifetimes is very strong. Finally, it could be argued that since this sample includes both DA and non-DA white dwarfs, appropriate cooling sequences should be used for each spectral type. However, the errors introduced by using inappropriate cooling sequences (that is cooling sequences for He-dominated white dwarf envelopes) in the calculation of the cooling times of DA white dwarfs are small when compared to the errors introduced in dating white dwarfs by poor mass estimates. Therefore, the temporal characteristics of the white dwarf population from them derived should be viewed with some caution. Note as well that there is not any guaranty that the sample of Sion et al. (1988) is representative of the whole population of white dwarfs, since it is by no means complete, and therefore some cautions are required when drawing conclusions. To be more precise, the sample of Sion et al. (1988) has very few low luminosity white dwarfs. In fact, this sample contains only twelve white dwarfs belonging to the low luminosity sample of Liebert et al. (1988), of which only four have mass, tangential velocity, and effective temperature determinations. Therefore, we have added to this sample — hereinafter “observational” sample — three additional white dwarfs of the sample of Liebert et al. (1988) for which a mass estimate could be found (Díaz-Pinto et al. 1994). Nevertheless, this

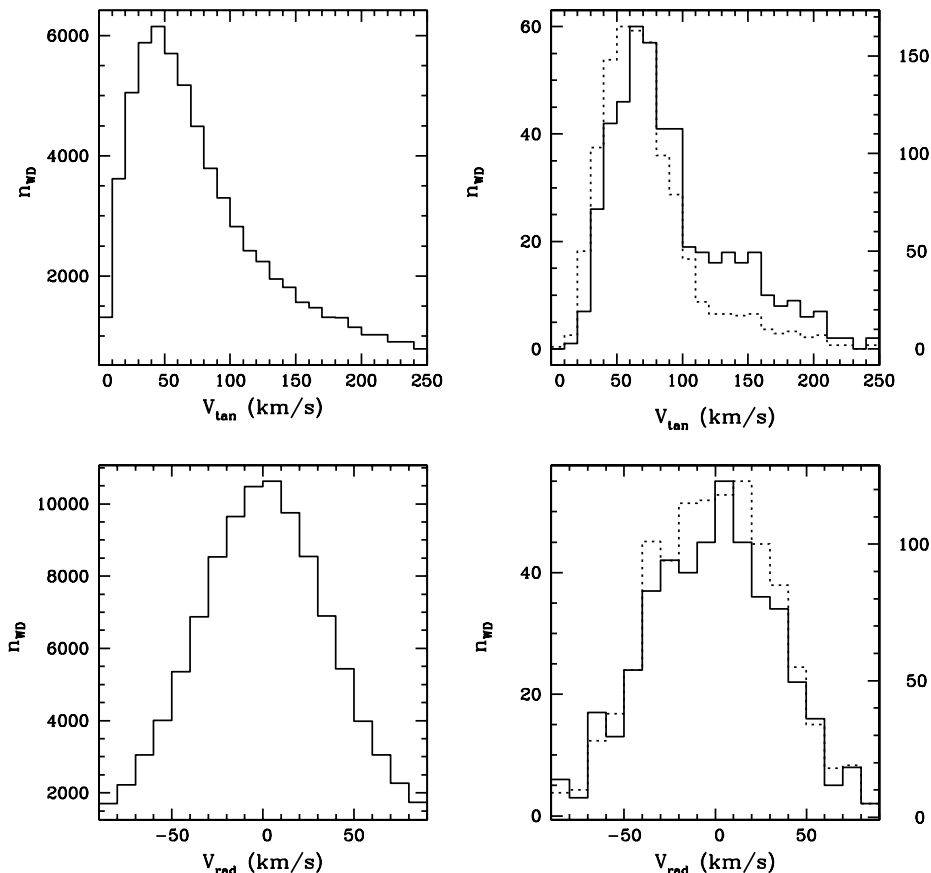


**Figure 2.** Tangential (upper left panel) and radial (lower left panel) velocity distributions for the original sample and the corresponding distributions for the restricted sample (upper and lower right panels, respectively). Also shown as dotted lines are the tangential and radial velocity distributions of the restricted sample with a looser restriction in proper motions (see text for details).

sample provides a unique opportunity to test the results obtained from a simulated white dwarf sample.

### 3.1 The overall kinematical properties of the samples

First we compare the overall kinematical properties of the white dwarf simulated samples with those of the observational sample, regardless of the birth time of their progenitors. In Figure 2 we show the distributions of the tangential and radial velocities for both the original and the restricted sample. The tangential velocity distribution of the original sample is shown in upper left panel of figure 2 and the tangential velocity distribution of the restricted sample is shown as a solid line (left scale) in the upper right panel. The restricted sample, which is kinematically selected, has a smaller tangential velocity dispersion ( $\sigma_{\text{tan}} \sim 80 \text{ km s}^{-1}$ ) than the original sample ( $\sigma_{\text{tan}} \sim 100 \text{ km s}^{-1}$ ). Here we have defined for operational purposes only the dispersions to be as the full width at half maximum of the distributions. Moreover, both samples are peaked at different tangential velocities: at  $V_{\text{tan}} \sim 45 \text{ km s}^{-1}$  for the original sample and at  $V_{\text{tan}} \sim 65 \text{ km s}^{-1}$  for the restricted sample, showing clearly that the restricted sample is biased towards larger tangential velocities, as it should be for a proper motion selected sample. In fact the most probable tangential velocity of the

restricted sample is almost one third larger than that of the total sample of white dwarfs. This kinematical bias is clearly seen as well in the behavior of the distribution at low tangential velocities where the restricted sample shows a deficit of low velocity stars, as expected from a kinematically selected sample. Note as well the existence of an extended tail at high tangential velocities, indicating the presence of high proper motion white dwarfs. Of course, all these effects are simply due to the selection criteria and, in particular to the assumed restriction in proper motion. The distribution of radial velocities of the original sample is shown in the lower left panel of figure 2 and the radial velocity distribution of the restricted sample is shown as a solid line (left scale) of the lower right panel. Both distributions have similar dispersions ( $\sigma_{\text{rad}} \sim 90 \text{ km s}^{-1}$ ) and both are well behaved and centered at  $V_{\text{rad}} = 0$ , as it should be since there is not any constrain on the radial velocities of the restricted sample.

In Figure 3 the tangential velocity distribution of the observational sample is shown. By comparing the tangential velocity distributions of figure 2 (upper panels) and figure 3 we can assure that the observational sample does not have a clear kinematical bias since it does not show a clear deficit of low tangential velocity white dwarfs — the ratio between the height of the peak and the height of the lowest velocity bin is the same for both the original sample and the observational sample: roughly 1/4 — and does not have an

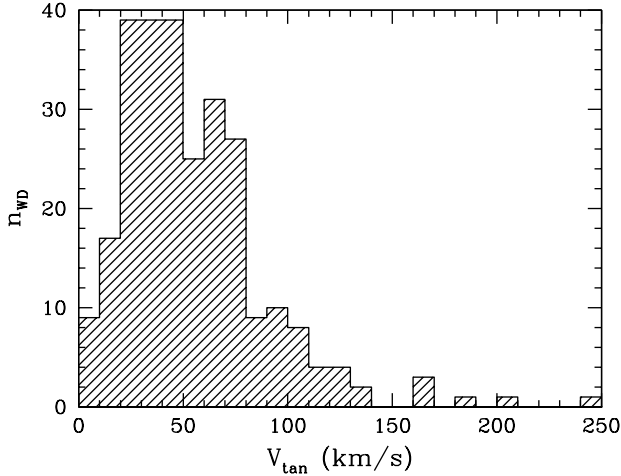


**Figure 3.** Tangential velocity distribution of the sample of Sion et al. (1988).

extended tail at high tangential velocities as the restricted sample does. Moreover, the observational sample peaks at  $V_{\text{tan}} \sim 40 \text{ km s}^{-1}$ , whereas the original sample (which is not kinematically selected) peaks at a very similar tangential velocity ( $V_{\text{tan}} \sim 45 \text{ km s}^{-1}$ ). However the tangential velocity dispersion ( $\sigma_{\text{tan}} \sim 60 \text{ km s}^{-1}$ ) of the observational sample is roughly one-third smaller than that of the original sample. This might be due to the absence of low luminosity white dwarfs in the observational sample. Notice that intrinsically dim white dwarfs are selected on the basis of a large proper motion and, therefore, are expected to have, on average, larger tangential velocities, thus increasing the velocity dispersion. To check this assumption we have run our Monte Carlo code with a *looser* restriction on proper motions ( $\mu \geq 0.08'' \text{ yr}^{-1}$ ). The result is shown in the upper right panel of figure 2 as a dotted line (right scale). Although the number of selected white dwarfs increases from  $\sim 85$  to almost 250 the tangential velocity dispersion decreases from  $\sigma_{\text{tan}} \sim 80 \text{ km s}^{-1}$  to  $\sigma_{\text{tan}} \sim 60 \text{ km s}^{-1}$  in good agreement with the tangential velocity dispersion of the observational sample. A final test can be performed by imposing a *tighter* restriction on visual magnitudes ( $m_V \leq 15.5^{\text{mag}}$ ). The resulting sample is now smaller — 58 white dwarfs — as should be expected, whereas the tangential velocity dispersion decreases to  $\sigma_{\text{tan}} \sim 40 \text{ km s}^{-1}$  and the most probable tangential velocity remains almost unchanged ( $V_{\text{tan}} \sim 40 \text{ km s}^{-1}$ ). On the other hand the radial velocity distribution — dashed line and right scale in the lower right panel of figure 2 — is nearly indistinguishable from the previous sample, selected with a tighter restriction. Nevertheless, the differences between the observational sample and the simulated samples could be considered as minor. Therefore we conclude that the simulated population of white dwarfs is fairly representative of the real population of white dwarfs.

### 3.2 The temporal behavior of the samples

Up to this moment we have compared the global kinematical characteristics of the simulated samples with those of the sample of Sion et al. (1988), but one of the major advantages of this latter sample is that all the mass determi-

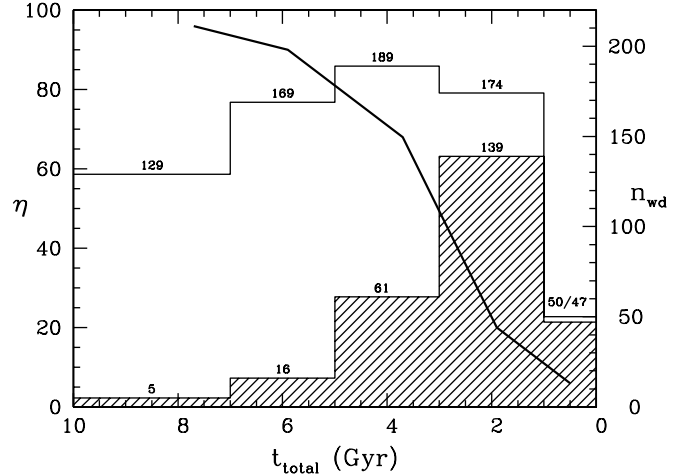


**Figure 4.** Time distributions of the restricted sample (non-shaded diagram) and the observational sample (shaded diagram) and percentage of missing white dwarfs in the observational sample. The total number of objects in each time bin is shown on top of the corresponding bin.

nations have been obtained using the same procedure, and consequently, in this sense, the sample is relatively homogeneous. Therefore, we can tentatively obtain the temporal variations of the kinematical properties as a function of the birth time of the progenitors of the white dwarfs belonging to the observational sample, and compare them with those of the simulated samples.

To this regard, in Figure 4 we show the histograms of the distribution of the birth times of white dwarfs belonging to the observational sample (shaded histogram) and to the restricted sample (non-shaded histogram). The number of objects in each time bin is also shown on top of each bin of the histogram. Time runs backwards and, therefore, old objects are located at the left of the diagrams, whereas young objects contribute to the time bins of the right part of the diagrams. It is important to realize that old bins may include kinematical data coming from either bright, low-mass white dwarfs, or dim, massive white dwarfs. The time bins have been chosen in such a way that the distribution of white dwarfs in the observational sample is efficiently binned. The first bin in time corresponds to objects older than 7 Gyr and has only 5 objects, most of them corresponding to intrinsically faint objects belonging to the sample of Liebert et al. (1988). The last bin corresponds to objects younger than 1 Gyr. The remaining three bins are equally spaced in time and correspond to white dwarf progenitors with ages running from 1 to 7 Gyr in 2 Gyr intervals. All the bins have been centered at the average age of the objects belonging to them ( $\sim 7.7, 5.9, 3.7, 1.9$  and  $0.5$  Gyr, respectively).

Since the youngest time bin corresponds to intrinsically bright white dwarfs it is expected that this time bin is reasonably complete in the observational sample. Therefore we have chosen the total number of stars in the simulated samples in such a way that the restricted sample has a number of objects in the youngest time bin comparable with that of the observational sample. Since there is no clear restriction in the ages of white dwarfs belonging to the restricted sample, the statistical reliability of the remaining time bins

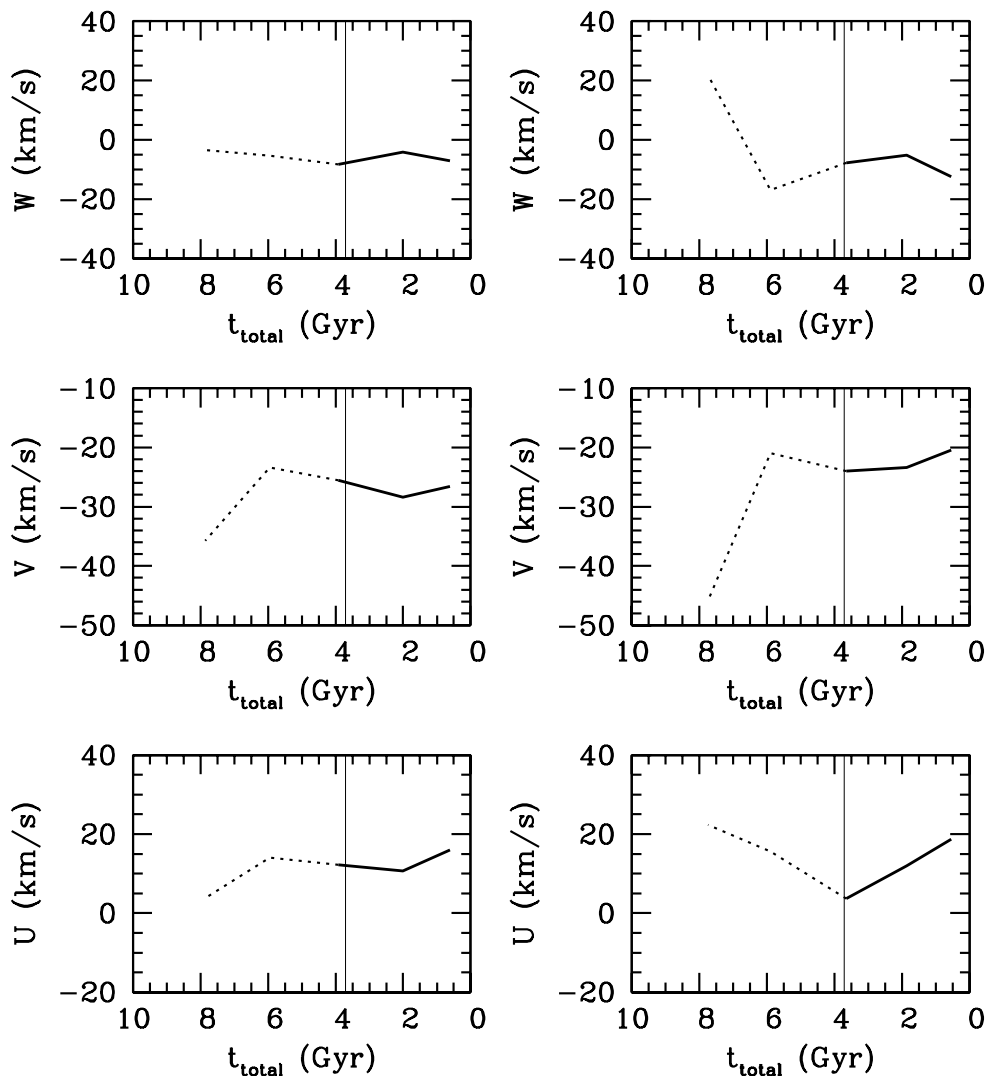


**Figure 5.** Components of the tangential velocity as a function of the birth time of the white dwarf progenitors for the restricted (left-hand panels) and the observational sample (right-hand panels), see text for details.

of the observational sample can be readily assessed. Note the huge difference in the number of white dwarfs between the observational sample and the restricted sample for the oldest time bins of figure 4. Clearly, the completeness of the observational sample decreases dramatically as the birth time increases. The percentage of missing white dwarfs ( $\eta$ ) in the observational sample as a function of the birth time of their corresponding progenitors is also shown in figure 4 as a solid line, assuming that the youngest time bin of the restricted sample is complete. We have considered the observational sample to provide reasonable estimates of the temporal variations of the velocity when one third of the expected number of white dwarfs is present in the corresponding time bin. This roughly corresponds to birth times smaller than 3.7 Gyr. Therefore, the only time bins that we

are going to consider statistically significant are the youngest three bins.

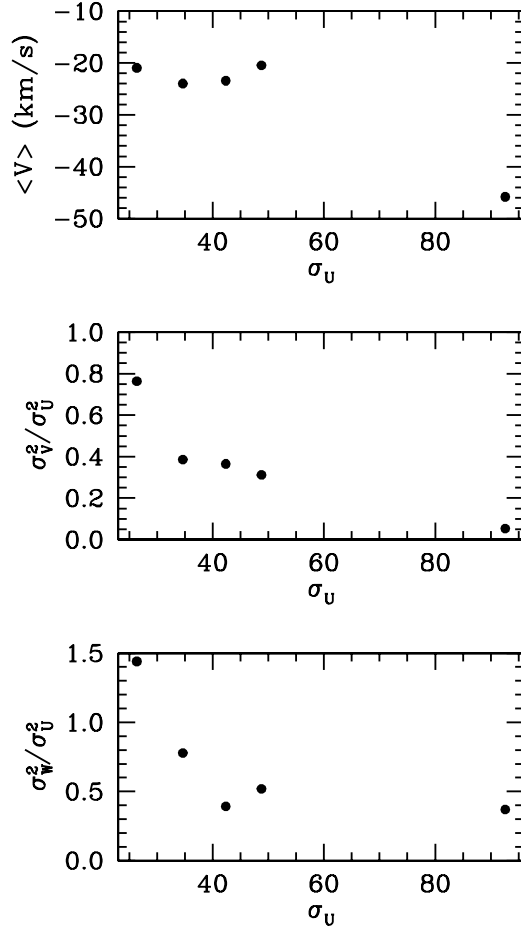
In Figure 5 we show as solid lines the temporal variation of the components of the tangential velocity as a function of the total age (white dwarf cooling age plus main sequence lifetime of the corresponding parent star) of white dwarfs belonging to the restricted sample (left-hand panels), and the same quantities for white dwarfs belonging to the observational sample (right-hand panels). Although we have not considered the data for  $t_{\text{total}} > 3.7$  Gyr to be reliable due to the incompleteness of the observational sample, we also show the temporal variations of all the three components of the tangential velocity for these times as dotted lines for the sake of completeness. The thinner vertical line corresponds to  $t_{\text{total}} = 3.7$  Gyr. As can be seen in this figure, the general trend for young objects is very similar for both samples. In

**Table 1.** Average values of the three components of the tangential velocity and their corresponding dispersions (both in  $\text{km s}^{-1}$ ) for several choices of  $z_f$  (in kpc).

$z_f$	$\langle U \rangle$	$\langle V \rangle$	$\langle W \rangle$	$\langle \sigma_U \rangle$	$\langle \sigma_V \rangle$	$\langle \sigma_W \rangle$
0.05	11.93	-13.87	-3.54	12.33	7.43	8.03
0.10	12.77	-16.60	-5.42	20.42	11.09	10.85
0.20	12.00	-19.86	-4.02	27.84	15.25	16.06
0.30	9.40	-24.95	-5.16	31.52	19.54	20.70
0.40	10.13	-24.93	-7.33	36.57	21.40	24.08
0.50	9.34	-27.77	-7.70	41.38	26.75	24.74
0.60	11.45	-29.90	-5.83	41.92	26.98	30.63

particular both the restricted and the observational sample have negative velocities across the galactic plane with velocities of  $W \sim -10 \text{ km s}^{-1}$ , both samples lag behind the sun with similar velocities of  $V \sim -25 \text{ km s}^{-1}$  and  $-20 \text{ km s}^{-1}$ , respectively, and both samples have positive radial velocities of roughly  $U \sim 20 \text{ km s}^{-1}$ . Finally, old objects in both samples lag behind the sun (middle panels) being the lag velocity comparable for both samples:  $V \sim -20 \text{ km s}^{-1}$  and  $-25 \text{ km s}^{-1}$ , respectively. Moreover, we have computed the time-averaged values of the velocities shown in figure 5 and we have found  $\langle U \rangle \sim 10$  and  $12 \text{ km s}^{-1}$ ,  $\langle V \rangle \sim -28$  and  $-23 \text{ km s}^{-1}$ , and  $\langle W \rangle \sim -8$  and  $-7 \text{ km s}^{-1}$ , respectively. We have computed as well the time-averaged values of the velocity dispersions for the restricted and the observational samples:  $\langle \sigma_U \rangle \sim 41$  and  $42 \text{ km s}^{-1}$ ,  $\langle \sigma_V \rangle \sim 27$  and  $30 \text{ km s}^{-1}$ , and  $\langle \sigma_W \rangle \sim 25$  and  $25 \text{ km s}^{-1}$ , and we have found that they are also in good agreement.

As already noted in §2, the most important ingredient needed to fit adequately the kinematics of white dwarfs is the exact shape of the scale height law. In fact, the luminosity function (see section 4 below) is only sensitive to the ratio of the initial to final scale heights ( $z_i/z_f$ ) of the disk and to the time-scale of disk formation ( $\tau_h$ ) but not to the exact value of say  $z_f$ . However when the kinematics of the sample are considered the reverse is true. That is the kinematics of the simulated samples are very sensitive to the exact value adopted for the final scale height. This is clearly illustrated in Table 1, where the time-averaged values for the three components of the tangential velocity and the tangential velocity dispersions are shown for several choices of the final scale height, but keeping constant the above mentioned ratio. As it can be seen there, the time-averaged radial component of the tangential velocity,  $\langle U \rangle$ , and the time-averaged perpendicular component of the tangential velocity,  $\langle W \rangle$ , are not very sensitive to the choice of  $z_f$ , whereas the time-averaged lag velocity is very sensitive to its choice. Regarding the velocity dispersions all three components are sensitive. We have chosen the value of  $z_f$  which best fits the average values of the observed sample. In order to produce the results of figures 4 and 5 a value of 500 pc was adopted for  $z_f$ , which is typical of a thick disk population. It is important to point out here that increasing (decreasing)  $z_f$  by a factor of two without keeping constant the ratio ( $z_i/z_f$ ) doubles (halves)  $\sigma_W$  for objects in the youngest time bin, which is the most reliable one, thus making incompatible the simulated and the observational samples. Similarly, increasing  $\tau_h$  by a factor of two changes dramatically the behaviour of the lag velocity since it changes the value of  $V$  for objects in the youngest time

**Figure 6.** Overall kinematical properties of the observational sample.

bin from  $\sim -20$  to  $\sim -10 \text{ km s}^{-1}$ . We conclude that the proposed scale height law is not in conflict with the observed kinematics of the white dwarf population.

### 3.3 A final remark on the reliability of the samples

Finally, it is interesting to compare the results of a kinematical analysis of the observational sample with the predictions obtained from main sequence star counts as given by equation (2). In Figure 6 we show the correlations between the  $V$  component of the tangential velocity (top panel), the ratio  $\sigma_V/\sigma_U$  (middle panel), and the ratio  $\sigma_W/\sigma_U$  (bottom panel) as a function of the radial velocity dispersion  $\sigma_U$  obtained from the data of main sequence stars compiled by Sion et al. (1988). Except for the last bin the agreement between the data obtained from the white dwarf sample and the data obtained from main sequence stars is fairly good ( $\sigma_V^2/\sigma_U^2 \sim 0.3$ ,  $\sigma_W^2/\sigma_U^2 \sim 0.5$  and  $V/\sigma_U^2 \sim -20$ ). However, it should be taken into account that the data coming from the last bin is obtained, as previously mentioned, with only five stars. Moreover, all these objects belong to the low luminosity sample of Liebert et al. (1988), which is strongly biased towards large tangential velocities and, besides, sys-

**Table 2.** Average values of the three components of the tangential velocity and their corresponding dispersions (both in  $\text{km s}^{-1}$ ) for the Monte Carlo simulation, the observational sample, and the Edvardsson et al. (1993) sample.

Sample	$\langle U \rangle$	$\langle V \rangle$	$\langle W \rangle$	$\langle \sigma_U \rangle$	$\langle \sigma_V \rangle$	$\langle \sigma_W \rangle$
MC	10	-28	-8	41	27	25
WD	12	-23	-7	42	30	25
E93	14	-21	-8	39	29	23

tematic errors affecting either mass and radius determinations or luminosity determinations (the bolometric corrections adopted in the latter work are highly uncertain) can mask the true behavior of the sample.

A final test of the validity of the assumptions adopted in this paper to derive the simulated populations can be performed by comparing the results of this section with the kinematical analysis of a sample of main sequence F and G stars (Edvardsson et al. 1993). These authors measured distances, proper motions and radial velocities (among other data) for a sample of 189 F and G stars. They also assigned individual ages for all the stars in the sample from fits in the  $T_{\text{eff}} - \log g$  plane. The same sample has been re-analyzed very recently by Ng & Bertelli (1998), using distances based on *Hipparcos* parallaxes and improved isochrones. We refer the reader to the latter work for a detailed analysis of the errors and uncertainties involved in dating individual objects. Although an analysis similar to that performed in §3.2 can be done, for the sake of conciseness we will only refer here to the average values of the three components of the tangential velocity and its corresponding dispersions. For this purpose in Table 2 we show the averaged values of the three components of the *tangential velocity* and their corresponding dispersions for the restricted sample of our Monte Carlo simulation, labelled MC, the observational sample, labeled WD, and the three components of the *velocity* and their dispersions for the Edvardsson et al. (1993) sample, labeled E93. As already discussed in §3.2 the agreement between the Monte Carlo simulation and the observational sample is fairly good. The comparison of both samples with the sample of Edvardsson et al. (1993) reveals that the agreement between the average values of the three samples is remarkably good, even if the dating procedure for individual objects is very different in both observational samples. The same holds for the averaged values of the three velocity dispersions. We conclude that our equation (2) represents fairly well the kinematical properties of the observed white dwarf population.

## 4 THE WHITE DWARF LUMINOSITY FUNCTION

### 4.1 The spatial distribution and completeness of the simulated white dwarf population

The  $1/V_{\text{max}}$  method (Schmidt 1968, Felten 1976), when applied to our simulated white dwarf population, should provide us with an unbiased estimator of its luminosity function, presumed completeness of the simulated samples in both proper motion and apparent magnitude, and provided

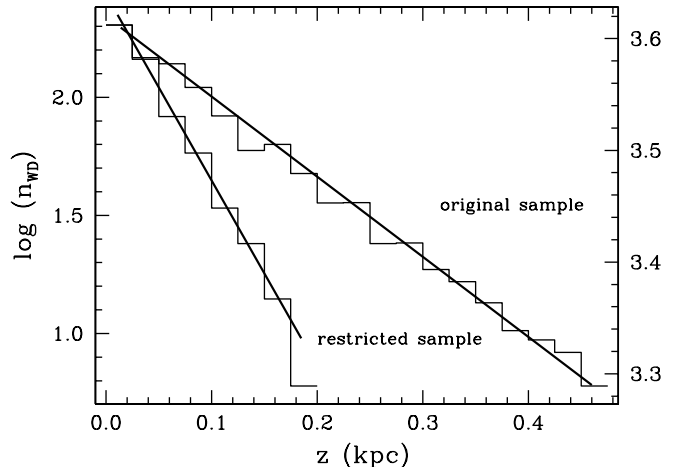


**Figure 7.** Histogram of the  $z$  distribution for both the original sample (right scale) and the restricted sample (left scale).

that the spatial distribution of white dwarfs is homogeneous. Strictly speaking this means that the maximum distance at which we find an object belonging to the sample is independent of the direction. In our case this is clearly not true — and, most probably, for a real sample this would certainly be the case as well — since we have derived the simulated samples assuming an exponential density profile across the galactic plane. Since the scale height law exponentially decreases with time (see §2) it is difficult to say “a priori” which is the final spatial configuration of the simulated white dwarf samples introduced in the previous sections.

In the histogram of Figure 7 we show the logarithmic distribution of the number of white dwarfs as a function of the absolute value of the  $z$  coordinate for both the original sample (right scale) and the restricted sample (left scale). Clearly, both distributions correspond to exponential disk profiles with different scale heights. Also shown in figure 7 are the best fits to these distributions. The corresponding scale heights from them derived are  $\approx 1.3$  kpc for the original sample, which is typical of a thick disk population, and considerably smaller  $\approx 129$  pc for the restricted sample which can be considered typical of a thin disk population. This is not an evident result since, as has been explained in §2, the simulated populations take naturally into account the fact that old objects are distributed over larger volumes (that is, with larger scale heights and therefore with larger velocity dispersion perpendicular to the plane of the galaxy) than young ones. Therefore, one could expect that the final spatial distribution of the restricted white dwarf population — which is kinematically selected — should reflect properties of an intermediate thin-thick disk population and certainly this is not the case. Obviously, since there is not any restriction in the distances (within the local column) at which a white dwarf belonging to the original sample can be observed the expected final scale height for this sample should be much larger, in good agreement with the simulations. Regarding the restricted sample, our results clearly indicate that we are selecting for this sample white dwarfs lying very close to the galactic plane. Moreover, if we change by a factor of two  $z_f$  as explained in §3, the final scale height of the restricted sample does not change appreciably and, on

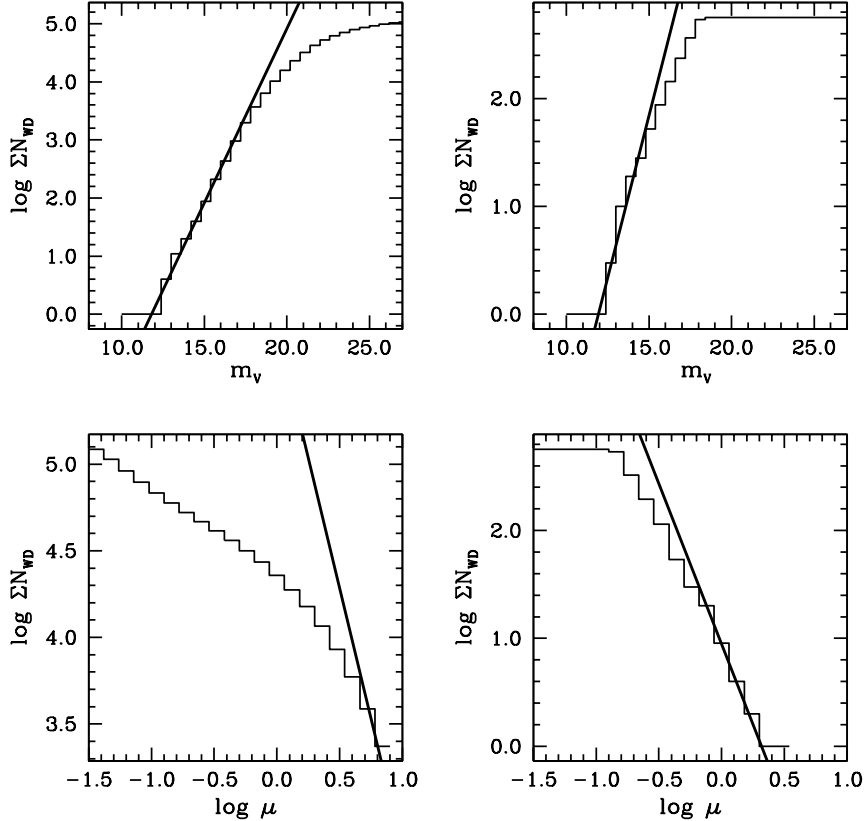


**Figure 8.** Cumulative histograms of apparent magnitude and proper motion for both the original and the restricted sample. See text for details.

the other hand, the dispersion of velocities perpendicular to the galactic plane does not agree with its observed value. Therefore, the final scale height of the restricted sample is clearly dominated by the selection criteria. It is important to realize that this scale height, taken at face value, is not negligible at all when compared with the value of the maximum distance at which a parallax is likely to be measured with relatively good accuracy — which is typically 200 pc — and which imposes an additional selection criterion (see §2) for white dwarfs belonging to the restricted sample, which are the white dwarfs which are going to be used in the process of determination of the white dwarf luminosity function. Therefore, the  $1/V_{\max}$  method must be generalized to take into account a space-density gradient. For this reason we have used the density law of figure 7 to define a new density-weighted volume element  $dV' = \rho(z) dV$  (Felten 1976; Avni & Bahcall 1980; Tinney, Reid & Mould 1993), being  $\rho(z)$  the density law derived from figure 7. This new, corrected, estimator provides a more accurate determination of the white dwarf luminosity function and, ultimately, a more realistic value of the space density of white dwarfs. All in all, for reasonable choices of a scale height law its effects on the derived white dwarf luminosity function in principle cannot be considered negligible.

The second, and probably more important issue, is the completeness of the samples used to build the white dwarf luminosity function. This is a central issue since the  $1/V_{\max}$

method assumes completeness of the samples. The reader should keep in mind that *the original sample is complete by construction*, since it consists of all white dwarfs generated by the Monte Carlo code, regardless of their distance, proper motion, apparent magnitude and tangential velocity; whereas the restricted sample is built with white dwarfs culled from the original sample according to a set of selection criteria and, therefore, its completeness remains to be assessed.

In Figure 8 we explore the completeness of the simulated samples. For this purpose, the cumulative star counts of white dwarfs with apparent magnitude smaller than  $m_v$  for the original sample are shown in the top left panel of figure 8, whereas the corresponding diagram for the restricted sample is shown in the top right panel. Also shown in figure 8 are the cumulative star counts of white dwarfs with proper motions larger than  $\mu$  belonging to the original sample (bottom left panel) and to the restricted sample (bottom right panel). For a complete sample distributed according to a homogenous spatial density, the logarithm of the cumulative star counts of white dwarfs with apparent magnitude smaller than  $m_v$  are proportional to  $m_v$  with a slope of 0.6 (see, for instance, Mihalas & Binney 1981). We also show in the top panels of figure 8 a straight line with such a slope. It is evident from the previous discussion that our samples are not, by any means, distributed homogeneously. Note as well that the effects of a scale height law are tangled in the stan-

dard test of completeness of the samples. Nevertheless, the effects of a scale height law can be disentangled since they should be quite apparent in the cumulative star counts diagram of the original sample, which is complete. A look at the top left panel of figure 8 reveals that the effects of the scale height law are evident for surveys with limiting magnitude  $m_V \gtrsim 19^{\text{mag}}$ . Therefore, we can now assess the completeness in apparent magnitude of the restricted sample, since the turn-off for this sample (see top right panel of figure 8) occurs at  $m_V \sim 17^{\text{mag}}$ . Consequently, the effects of the scale height law can be completely ruled out, and this value can be considered as a safe limit for which the restricted sample is complete in apparent magnitude.

The completeness of the restricted sample in proper motion can be assessed in a similar way. Again, the assumption of an homogenous and complete sample in proper motion leads to the conclusion that the logarithm of the cumulative star counts of white dwarfs with proper motion larger than  $\mu$  should be proportional to  $\mu$  with a slope of  $-3$  (see, for instance, Oswald & Smith 1995, and Wood & Oswald 1998). A look at the bottom left panel of figure 8 reveals that for the original sample this is not by far the case. In other words, since this particular sample is complete by construction the hypothesis of an homogenous distribution of proper motions must be dropped. This is again one, and probably the most important, of the effects associated with a scale height law since the kinematics of the samples are highly sensitive to the choice of the scale height law (see §2, equation (2) and table 1). It is important to realize that the effects of a scale height law are more prominent in proper motion than in the spatial distribution and this can be directly checked for a real sample, thus providing a direct probe of the history of the star formation rate per unit volume. Finally, in the lower right panel of figure 8 the cumulative star counts in proper motion of white dwarfs belonging to the restricted sample are shown. As expected, the effects of a scale height law are in this case negligible since we are culling white dwarfs with high proper motion for which the original sample is reasonably complete (see the lower left panel of figure 8). The exact value of the turn-off is in this case  $\mu \sim 0.3'' \text{ yr}^{-1}$ , in close agreement with the results of Wood & Oswald (1998).

It is quite clear from the previous discussions that one of the ingredients that has proven to be essential in the determination of the white dwarf luminosity function is the adopted scale height law. In principle one should expect two kinds of competing trends. On the one hand, the effects of the scale height law should be more dramatic for old objects, because old objects have a larger velocity dispersion (although the effects of a spatial inhomogeneity should be, as well, less apparent) and the tail of the white dwarf luminosity function is populated predominantly by this kind of white dwarfs (intrinsically dim, high proper motion objects). Therefore, one should expect that the cut-off in the white dwarf luminosity function is influenced either by the spatial distribution of white dwarfs or by their velocity distribution or by a combination of both. On the other hand, objects populating the tail of the luminosity function are intrinsically dim objects and, therefore, in order to be selected for the restricted sample they must be close neighbors. This, in turn, implies that the average distance at which we are looking for white dwarfs is small and, consequently, the effects of a scale height law should be less apparent. The reverse is true

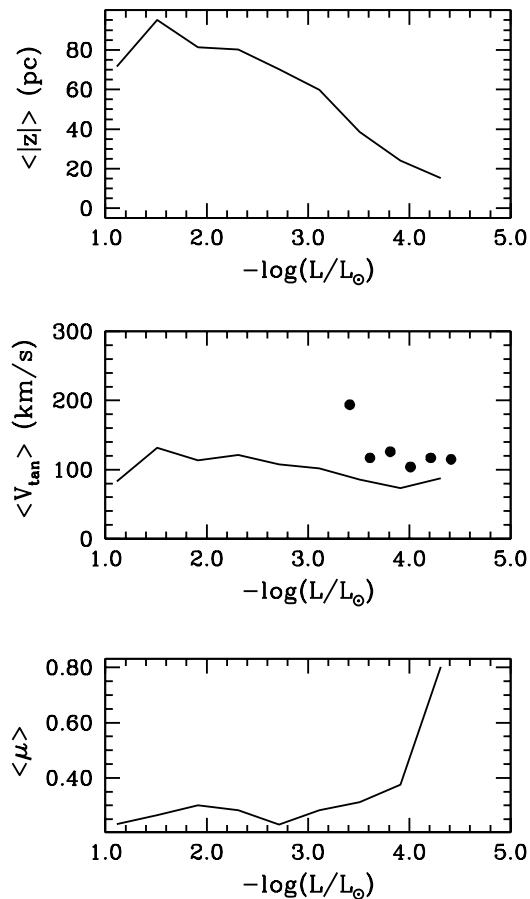


**Figure 9.** Average properties of the restricted sample as a function of the luminosity. Bottom panel: average  $z$  coordinate of white dwarfs of the restricted sample; middle panel: average tangential velocity for these white dwarfs, the observational data has been taken from Liebert et al. (1988); and top panel: average proper motion of these objects.

at moderately high luminosities. Therefore it is interesting to see which are the dominant effects as a function of the luminosity. For this purpose, in Figure 9 we show several average properties of white dwarfs belonging to the restricted sample as a function of their luminosity for a typical Monte Carlo simulation.

In the top panel of figure 9 we show the average distance to the galactic plane of white dwarfs belonging to the restricted sample. As it can be seen, the average distance to the galactic plane of intrinsically bright white dwarfs can be as high as 100 pc, which is a sizeable fraction of the derived scale heights of the white dwarf samples. Consequently we expect that the effects of an inhomogeneous spatial distribution should be very prominent at high luminosities. Conversely, the average distance to the galactic plane for white dwarfs near the observed cut-off in the white dwarf luminosity function is only  $\sim 10$  pc. Therefore as the luminosity decreases we are probing smaller volumes and the effects of an inhomogeneous *spatial* distribution at low luminosities are expected to be, from this point of view, small (but see, however, the discussion in §4.4).

In the middle panel of figure 9 the average tangential velocity of objects belonging to the restricted sample is shown

as a function of the luminosity. The observational data is shown as solid circles and has been obtained from Liebert et al. (1988). Their adopted restriction in proper motion  $\mu_0 = 0.80'' \text{ yr}^{-1}$  is significantly larger than the one we adopt here  $\mu_0 = 0.16'' \text{ yr}^{-1}$ , which is consistent with the cut-off in proper motion adopted by Oswalt et al. (1996). Therefore we expect a smaller average tangential velocity. The agreement is fairly good since, given the ratio of proper motion cut-offs, the average tangential velocity of our restricted sample should be roughly a 20% smaller: a closer look at the middle panel of figure 9 shows that the average tangential velocity reported by Liebert et al. (1988) is  $\sim 120 \text{ km s}^{-1}$ , whereas we obtain  $\sim 90 \text{ km s}^{-1}$ . These figures reinforce the general idea that our simulations are fully consistent with the observed kinematics of the white dwarf population.

Finally, in the bottom panel of figure 9 the average proper motion distribution of those stars belonging to the restricted sample is shown as a function of the luminosity. As it can be seen there, low luminosity white dwarfs belonging to the restricted sample have, on average, large proper motions. As expected from the discussion of the two previous panels, the distribution of proper motions is smoothly increasing for luminosities in excess of  $\sim 10^{-3} L_{\odot}$ : since the average value of the tangential velocity remains approximately constant, and we are selecting objects with smaller average distances, the net result is an increase in the average proper motion. Moreover, white dwarfs belonging to the low luminosity portion of the white dwarf luminosity function are preferentially culled from the original sample because of their high proper motion. That is the same to say that the selection criterion is primarily the proper motion one and that the criterion on apparent magnitude has little to do for these luminosities, in agreement with the results of Wood & Oswalt (1988). As a final consequence the effects of an inhomogeneous distribution in *proper motions* will be more evident at high luminosities, where the average proper motion is smaller (see the discussion of the lower left panel of figure 8). All in all, the effects of the inhomogeneities in both proper motion and  $z$  will be more prominent at high luminosities, where the observational luminosity function already takes into account these effects (Fleming et al. 1986).

## 4.2 The Monte Carlo simulated white dwarf luminosity functions

In Figure 10 we show a set of panels containing the white dwarf luminosity functions obtained from ten different Monte Carlo simulations. That is the same to say that ten different initial seeds were chosen for the random number generator and, consequently, ten *independent realizations* of the white dwarf luminosity function were computed (in fact, we have computed twenty independent realizations, of which only ten are shown in figure 10). The adopted age of the disk was  $t_{\text{disk}} = 13 \text{ Gyr}$  and the set of restrictions used to build the sample is that of §2, which is the same set used by Oswalt et al. (1996) to derive their observational white dwarf luminosity function. The simulated white dwarf luminosity functions were computed using a generalized  $1/V_{\text{max}}$  method (Felten 1976; Tinney et al. 1993; Qin & Xie 1997) which takes into account the effects of the scale height. The error bars of each bin were computed according to Liebert et al. (1988): the contribution of each star to the total error

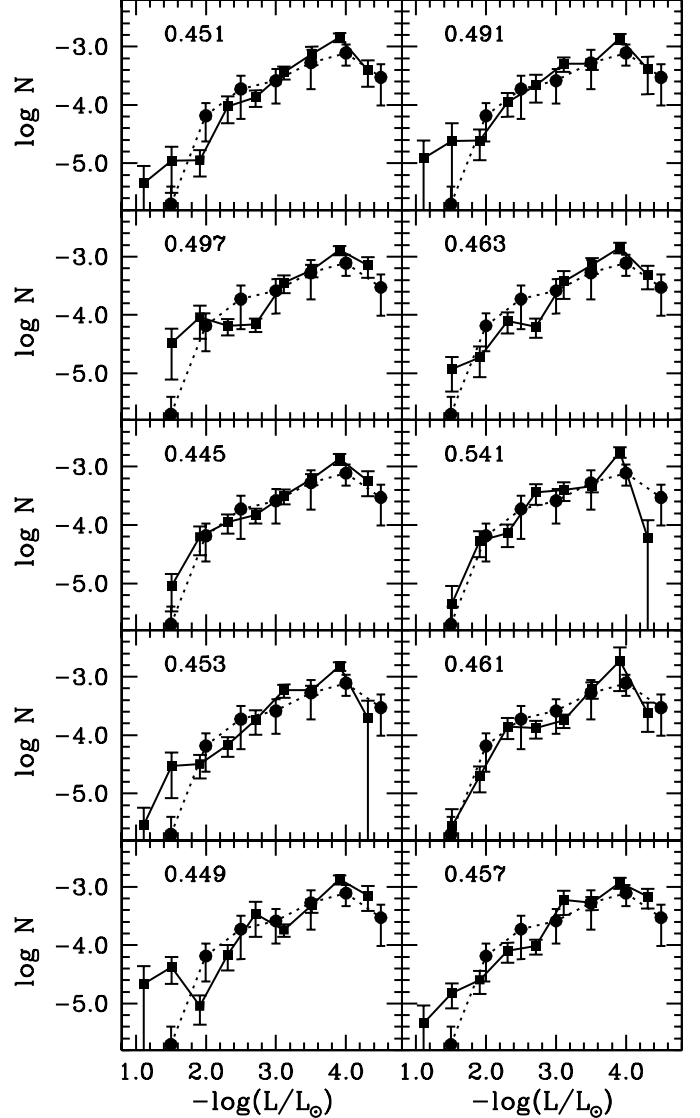


**Figure 10.** Panel showing different realizations of the simulated white dwarf luminosity function — filled squares and solid lines — compared to the observational luminosity function of Oswalt et al. (1996) — filled circles and dotted line.

budget in its luminosity bin is conservatively estimated to be the same amount that contributes to the resulting density; the partial contributions of each star in the bin are squared and then added, the final error is the square root of this value. The resulting white dwarf luminosity functions are plotted as solid squares; a solid line linking each one of their points is also shown as a visual help. Also plotted in each one of the panels is the observational white dwarf luminosity function of Oswalt et al. (1996), which is shown as solid circles linked by a dotted line. For each realization of the white dwarf luminosity function the value obtained for  $\langle V/V_{\text{max}} \rangle$  is also shown in the upper left corner of the corresponding panel. Finally, and for sake of completeness, the total number of objects in the restricted sample,  $N_{\text{WD}}$ , of the different realizations of the white dwarf population, and the distribution of objects,  $N_i$ , in each luminosity bin,  $i$ , of the Monte Carlo simulated white dwarf luminosity functions are shown

**Table 3.** Total number of white dwarfs,  $N_{\text{WD}}$ , and white dwarfs in each bin,  $N_i$ , for each of the twenty realizations of the simulated white dwarf luminosity functions.

$i$	$N_{\text{WD}}$	$N_1$	$N_2$	$N_3$	$N_4$	$N_5$	$N_6$	$N_7$	$N_8$	$N_9$
1	200	1	8	5	14	42	38	42	44	6
2	216	1	6	11	18	29	48	49	53	1
3	203	0	4	8	22	36	39	45	43	6
4	176	0	6	6	17	18	35	41	44	9
5	210	1	5	8	17	24	49	48	53	5
6	191	1	7	10	23	24	37	44	37	8
7	202	0	3	12	29	27	42	50	35	4
8	222	0	1	16	18	38	41	50	57	1
9	197	0	5	12	20	22	34	51	47	6
10	198	1	1	9	16	28	44	49	47	3
11	204	0	5	10	21	25	38	44	53	8
12	198	1	3	14	20	33	36	50	35	6
13	175	0	3	14	20	23	32	44	37	2
14	182	0	6	9	15	28	40	43	35	6
15	185	2	6	6	19	30	31	44	43	4
16	213	1	3	16	21	33	31	45	56	7
17	189	2	2	11	25	22	32	43	44	8
18	207	1	4	7	17	33	38	41	61	5
19	217	1	10	10	28	17	47	55	42	7
20	210	0	4	13	19	31	38	46	55	4

**Table 4.**  $\chi^2$  test of the compatibility of the Monte Carlo simulated samples.

$i$	2	3	4	5	6	7	8	9	10	11	12	13	14	15	16	17	18	19	20
1	0.24	0.80	0.21	0.41	0.37	0.05	0.03	0.16	0.24	0.33	0.32	0.04	0.70	0.86	0.17	0.06	0.75	0.02	0.34
2		0.46	0.09	0.93	0.26	0.31	0.59	0.48	0.79	0.48	0.30	0.37	0.36	0.47	0.29	0.11	0.67	0.19	0.86
3			0.40	0.69	0.81	0.78	0.22	0.73	0.69	0.88	0.90	0.44	0.89	0.85	0.67	0.56	0.81	0.16	0.89
4				0.63	0.86	0.13	0.01	0.81	0.20	0.88	0.19	0.24	0.77	0.60	0.14	0.57	0.36	0.37	0.26
5					0.65	0.35	0.16	0.80	0.90	0.92	0.38	0.26	0.68	0.65	0.39	0.43	0.90	0.54	0.84
6						0.77	0.01	0.92	0.32	0.89	0.86	0.59	0.94	0.85	0.44	0.89	0.32	0.83	0.49
7							0.11	0.68	0.52	0.47	0.89	0.80	0.55	0.34	0.27	0.61	0.11	0.42	0.50
8								0.12	0.67	0.11	0.23	0.20	0.03	0.06	0.46	0.04	0.31	0.01	0.76
9									0.58	0.99	0.77	0.82	0.77	0.68	0.77	0.83	0.53	0.59	0.92
10										0.54	0.69	0.58	0.54	0.57	0.45	0.51	0.74	0.07	0.81
11											0.56	0.41	0.72	0.67	0.85	0.81	0.87	0.46	0.95
12												0.79	0.84	0.67	0.77	0.77	0.29	0.15	0.71
13													0.62	0.51	0.38	0.60	0.15	0.10	0.63
14														0.79	0.24	0.38	0.40	0.25	0.56
15															0.47	0.65	0.82	0.16	0.61
16																0.78	0.79	0.04	0.96
17																	0.38	0.28	0.50
18																		0.04	0.93
19																			0.12

in Table 3. The total number of white dwarfs belonging to the restricted sample is roughly 200, which is the typical size of the samples used to build the currently available observational luminosity functions. This number is important since the assigned error bars are strongly dependent on the number of objects in each luminosity bin.

It is important to notice the overall excellent agreement between the simulated data and the observational luminosity function. However, there are several points that deserve further comments. The first one is that the simulated white dwarf luminosity functions are systematically larger than the observational luminosity functions for luminosities in excess of  $\log(L/L_{\odot}) = -2.0$ . This behavior reflects the effects of the spatial inhomogeneity of the simulated white dwarf

samples. It is important to realize that the hot portion of the white dwarf luminosity function of Oswalt et al. (1996) has been derived without taking into account the effects of a scale height, in contrast with the procedure adopted by Fleming et al. (1986), where those effects were properly taken into account. When one compares the luminosity functions obtained in this section with that of Fleming et al. (1986) the agreement is excellent. Also of interest is the fact that the hot portion of the white dwarf luminosity function varies quite considerably for the different realizations. The reason for this behavior is that at high luminosities the evolution is dominated by neutrino losses and it is fast. Therefore, the probability of finding such white dwarfs is relatively small and the statistical significance of those bins is

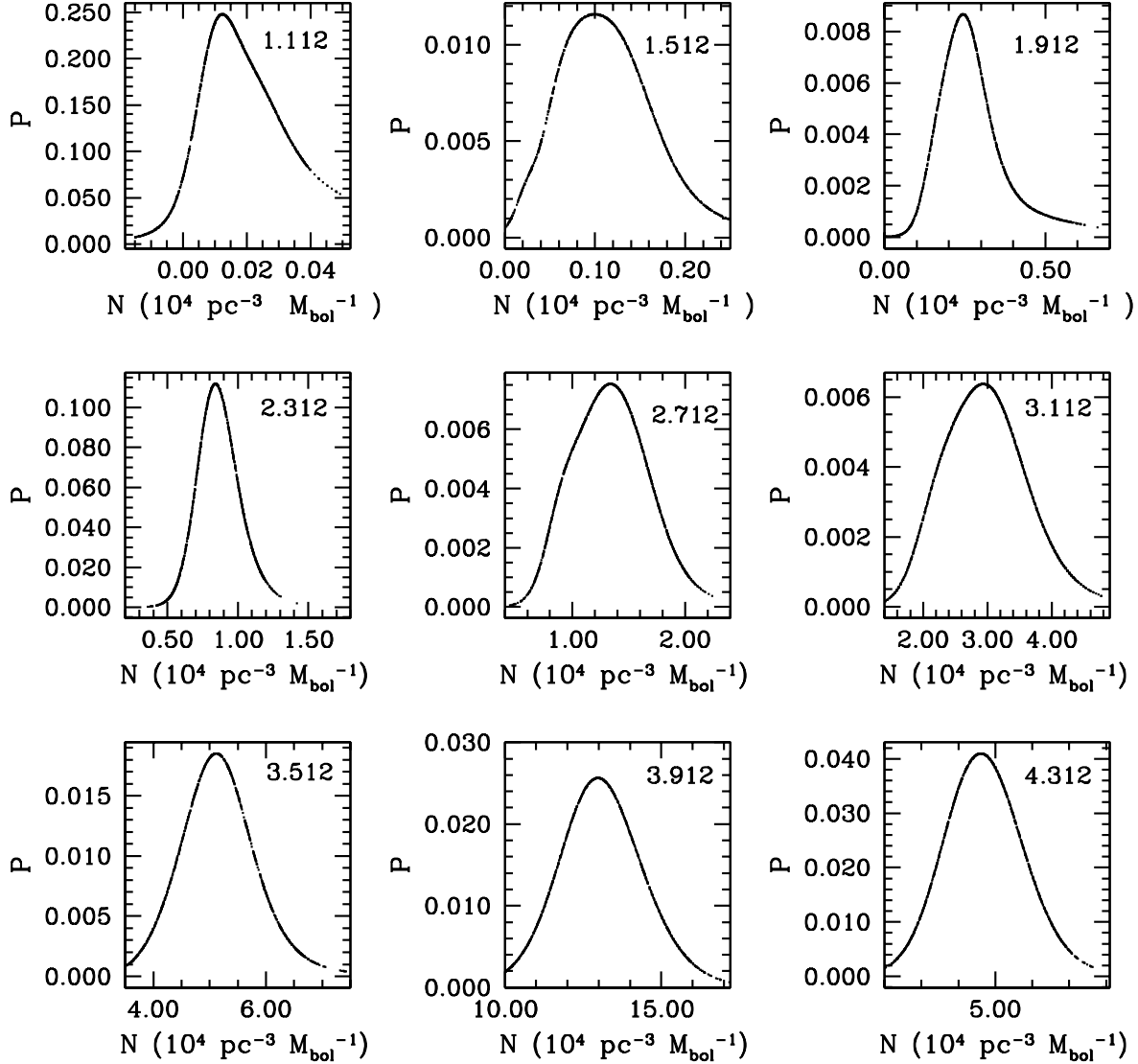


Figure 11. Probability distribution functions for each luminosity bin.

low. Consequently, the exact shape of the luminosity function at  $\log(L/L_{\odot}) \geq -3.0$  is strongly dependent of the initial seed of the pseudo-random number generator. This is further confirmed by comparing the second and the third column of table 3 where the total number of objects in the restricted sample and the number of objects in the first bin of the white dwarf luminosity function of each realization of the Monte Carlo simulations are shown. As a consequence the real error bars that should be assigned to each bin are presumably larger than those of figure 10. Moreover, any attempt to derive the volumetric star formation rate using data from the bins at high luminosities (Noh & Scalo, 1990) is based on very weak grounds. It is also important to notice that the completeness of the simulated samples as derived from the value of  $\langle V/V_{\max} \rangle$  is relatively large. In fact, for a complete and homogeneous sample this value should be equal to 0.5; since the simulated sample samples are not

homogenous the values obtained here can be considered as reasonable.

Finally, it is convenient to point out here that we have done a  $\chi^2$  test of the compatibility of the Monte Carlo simulated samples. The results are shown in Table 4, where the probability of an independent observer to find the realizations compatible is shown for each pair of realizations. As it can be seen, this probability can be as low as 0.01, which is the same to say that the corresponding luminosity functions are completely incompatible, even if they have derived from the same set of input parameters and selection criteria. Obviously, the conclusion is that for a reasonable number of objects in the restricted sample, the white dwarf luminosity function is dominated by the selection criteria.

**Table 5.** Error bars of the twenty independent realizations of the Monte Carlo simulated white dwarf luminosity functions in each luminosity bin and the same quantities for the Bayesian luminosity function (last row).

$i$	$\Delta \log(n_1)$	$\Delta \log(n_2)$	$\Delta \log(n_3)$	$\Delta \log(n_4)$	$\Delta \log(n_5)$	$\Delta \log(n_6)$	$\Delta \log(n_7)$	$\Delta \log(n_8)$	$\Delta \log(n_9)$
1	1.000	0.484	0.517	0.464	0.597	0.238	0.261	0.180	0.454
2	1.000	0.718	0.432	0.368	0.446	0.253	0.179	0.163	1.000
3	0.000	0.631	0.514	0.363	0.283	0.285	0.215	0.216	0.453
4	0.000	0.877	0.537	0.524	0.393	0.272	0.224	0.190	0.525
5	1.000	0.723	0.476	0.481	0.319	0.256	0.347	0.171	0.474
6	1.000	0.461	0.431	0.376	0.285	0.447	0.251	0.210	0.372
7	0.000	0.974	0.474	0.392	0.340	0.262	0.316	0.699	0.517
8	0.000	1.000	0.473	0.417	0.385	0.353	0.213	0.206	1.000
9	0.000	0.590	0.539	0.387	0.362	0.500	0.304	0.205	0.439
10	1.000	1.000	0.541	0.440	0.496	0.275	0.213	0.195	0.628
11	0.000	0.763	0.577	0.312	0.258	0.338	0.245	0.177	0.381
12	1.000	0.746	0.441	0.446	0.404	0.240	0.435	0.201	0.429
13	0.000	0.618	0.450	0.362	0.373	0.270	0.306	0.191	0.775
14	0.000	0.741	0.644	0.486	0.281	0.344	0.195	0.190	0.425
15	0.768	0.887	0.560	0.409	0.292	0.357	0.423	0.178	0.824
16	1.000	0.890	0.450	0.326	0.335	0.344	0.214	0.332	0.458
17	0.785	0.965	0.446	0.318	0.497	0.324	0.203	0.171	0.408
18	1.000	0.537	0.496	0.536	0.349	0.254	0.197	0.161	0.484
19	1.000	0.383	0.517	0.478	0.362	0.319	0.393	0.259	0.411
20	0.000	0.710	0.347	0.376	0.350	0.273	0.262	0.262	0.550
B	$^{+0.574}$ $_{-\infty}$	0.343	0.343	0.416	0.520	0.167	0.114	0.089	0.496

### 4.3 A bayesian analysis of the simulated samples

As previously stated, changing the initial seed of the random function generator the Monte Carlo code provides different independent realizations of the white dwarf luminosity function. All these realizations are “a priori” equally good. Besides, since the number of objects that is used to compute the white dwarf luminosity function is relatively small, large deviations are expected, especially at relatively high luminosities for which the cooling timescales are short. This, in turn, results in very probable underestimates of the associated uncertainties, especially at luminosities larger than  $\log(L/L_{\odot}) \gtrsim -3.0$ . Consequently we have used bayesian statistical methods (Press 1996) to obtain a realistic estimation of the errors involved and the most probable value of the density of white dwarfs for each luminosity bin.

The problem can be stated as follows: for a given luminosity,  $L$ , we want to know the most probable value of the white dwarf luminosity function,  $N$ , given a set of  $N_i$  simulations assuming that all simulations are equally good. To compute  $N$  one must maximize the probability distribution

$$P(N/N_i) \propto \prod_i \frac{1}{2} (P_{G_i} + P_{B_i}) \quad (3)$$

where  $P_G$  and  $P_B$  are the probability of being a good and a bad simulation, respectively. We can calculate them following closely Press (1996):

$$P_{G_i} = \exp \left[ -\frac{(N_i - N)^2}{2\sigma_i^2} \right] \quad (4)$$

$$P_{B_i} = \exp \left[ -\frac{(N_i - N)^2}{2S^2} \right]$$

where  $\sigma_i$  is the error bar of each bin of the luminosity function and  $S$  is a large but finite number characterizing the

maximum expected deviation in  $N_i$ . We recall that the contribution to the error of each white dwarf is equal to the inverse of its maximum volume squared.

The results are shown in Figure 11, where the probability distributions corresponding to each luminosity bin, computed with the previous method, are displayed. The logarithm of the luminosity of each bin in solar units is shown in the upper right corner of each panel. All the probability distributions, except that of the brighter luminosity bin, have a Gaussian profile. This is a direct consequence of the poor statistical significance of the first bin. In order to produce these probability distributions 20 independent realizations of the simulated samples were used. This is a reasonable number: increasing the total number of simulations does not introduce substantial improvements in the statistical significance of the first bin, which is the less significant. From these probability distributions a better estimate of the statistical noise can be obtained. We have estimated the resulting error bars by assuming a conservative 95% confidence level (approximately  $2\sigma$ ). In Table 5 we show the computed deviations for each of the twenty realizations of the Monte Carlo simulated white dwarf luminosity functions and the most probable error bars computed at the 95% confidence level. The error bars obtained from a bayesian analysis of the twenty Monte Carlo simulations compare favourably, roughly speaking, with those of each individual Monte Carlo simulation. However, for samples where the total number of white dwarfs is smaller than 200 (the simulations presented here) the errors for each of the luminosity bins are severe underestimates of the real errors, especially at low luminosities.

In Figure 12 the most probable white dwarf luminosity function — hereinafter bayesian white dwarf luminosity function — with its corresponding error bars is shown, obtained by maximizing the probability distributions of figure 11. Except for moderately high luminosities — i.e. for lumi-

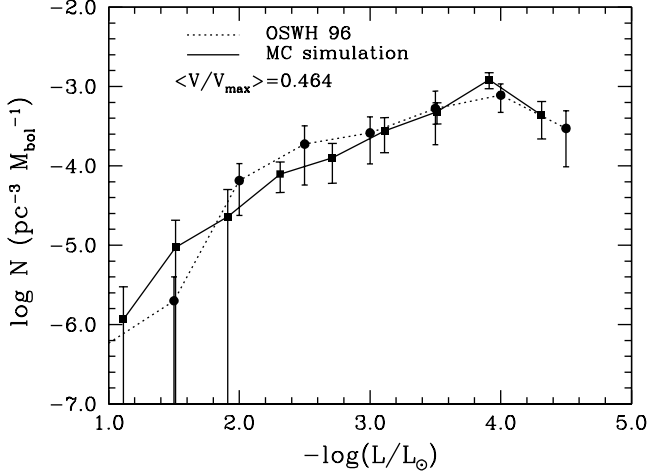


**Figure 12.** Bayesian luminosity function.

nosities larger than  $\log(L/L_{\odot}) = -2.0$  — where the effects of the spatial inhomogeneities are most obvious the agreement between the observational luminosity function and the bayesian luminosity function is excellent. Moreover, for the bayesian white dwarf luminosity we have computed a synthetic value of  $\langle V/V_{\max} \rangle$  as an average of the corresponding values for each of the twenty realizations with the weights given by the probability of each realization obtained from the probability distributions of figure 11. We have obtained a value of  $\langle V/V_{\max} \rangle = 0.464$  which remains close to the canonical value of  $\langle V/V_{\max} \rangle = 0.5$ , valid for an homogenous and complete sample.

#### 4.4 The age of the disk

Perhaps one of the most surprising results of the simulations presented here is the age of the disk itself. The value of 13 Gyr adopted in this paper fits nicely the observational data of Oswalt et al. (1996) as can be seen in figure 12. This a direct consequence of the adopted scale height law, since using the same set of cooling sequences and a conventional approach to compute the white dwarf luminosity function with a constant volumetric star formation rate, Salaris et al. (1997) derived an age for the solar neighborhood of 11 Gyr when the effect of phase separation upon crystallization was taken into account and of 10 Gyr when phase separation was neglected. Thus the ultimate reason of the increase in the adopted age of the solar neighborhood is not due to the details of the adopted cooling sequences. Instead, this increase can be easily explained in terms of the model of galactic evolution. We recall that the white dwarf luminosity function measures the number of white dwarfs per *cubic parsec* and unit bolometric magnitude. Therefore in order to evaluate it the volumetric star formation rate is required. In our case we can define the effective star formation rate per cubic parsec as  $\psi_{\text{eff}}(t) \approx \psi(t)/H_p(t)$ . With the laws adopted here for  $\psi(t)$  and  $H_p(t)$  it is easy to verify that the effective star formation rate only becomes significant after  $\sim 2$  Gyr (Isern et al. 1995a,b).

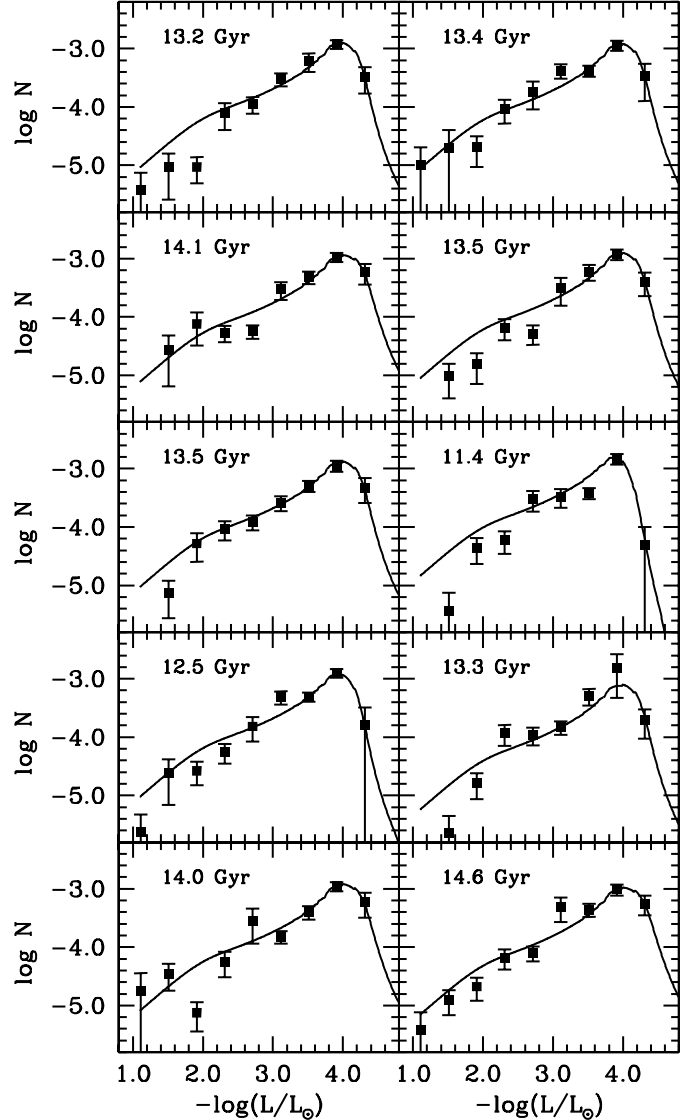


**Figure 13.** Panel showing different simulated luminosity functions (filled squares) and their corresponding fit using a standard method.

#### 4.5 Statistical uncertainties in the derived age of the disk

The easiest and more straightforward way to assess the statistical errors associated with the measurement of the age of the solar neighborhood is trying to reproduce the standard procedure. That is, we have fitted the position of the “observational” cut-off of each of the Monte Carlo realizations with a standard method (Hernanz et al. 1994) to compute the white dwarf luminosity function using *exactly* the same inputs adopted to simulate the Monte Carlo realizations, except, of course, the age of the disk, which is the only free parameter. The results are shown in Figure 13 for ten of the twenty realizations. As is usual with real observational luminosity functions the theoretical white dwarf luminosity functions were normalized to the bin with minimum error bars. The derived ages of the disk for each one of the realizations are shown in the upper left corner of the corresponding panel. As it can be seen, there is a clear bias:

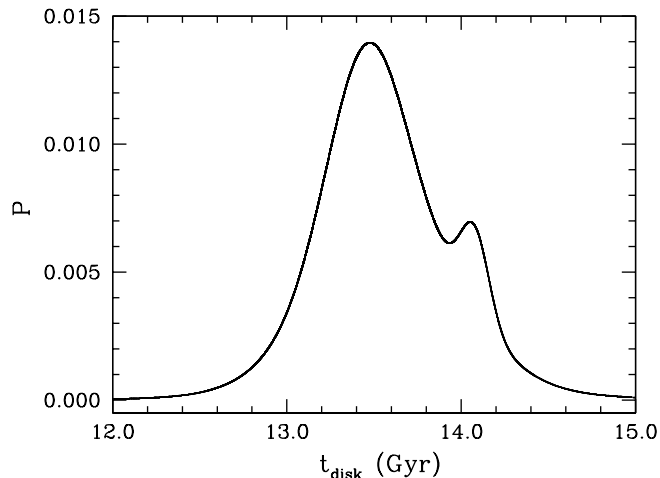


Figure 14. Bayesian analysis of the derived age of the disk.

the derived ages of the disk are *systematically* larger than the input age of the Monte Carlo simulator by about half a Gyr. This is a direct consequence of the binning procedure, since we are grouping white dwarfs belonging to the maximum of the white dwarf luminosity function in the lowest luminosity bin, and can be avoided by using the cumulative white dwarf luminosity function, which minimizes the effects of the binning procedure.

We have used the Bayesian inference techniques described in §4.3 to assign a purely statistical error to our age estimates. In order to do this we need to know a formal uncertainty for each one of the independent realizations. Since the value of  $\langle V/V_{\max} \rangle$  is a good measure of the overall quality of the sample (despite the fact that the samples are inhomogeneous) we have adopted  $\sigma_i = 2(0.5 - \langle V/V_{\max} \rangle) t_{\text{disk}}$ . The corresponding probability distribution is shown in Figure 14, which leads to a most probable age of the disk of  $t_{\text{disk}} = 13.5 \pm 0.8$  Gyr at the 95% confidence level ( $2\sigma$ ) which has to be compared with the adopted input age in our Monte Carlo simulation which was taken to be 13 Gyr. This uncertainty is in good agreement with the results of Wood & Oswalt (1998). If one relaxes the confidence level to  $1\sigma$  the associated error bar is  $\pm 0.4$  Gyr. It is nonetheless important to realize that there is a systematic increase in the inferred disk ages of  $\sim 5\%$ .

## 5 CONCLUSIONS

We have built a Monte Carlo code which has allowed us to reproduce quite accurately the process of building the white dwarf luminosity function from the stage of object selection and data binning. Our Monte Carlo simulation includes a model of galactic evolution based on well established grounds. The simulated samples obtained with our code reproduce very well the overall kinematical properties of the observed white dwarf population. We have explored as well the temporal evolution of such properties and we have found that there is a fair agreement between the observed distributions and the simulated ones. However, we have shown that observed sample has very few old white dwarfs and this has constrained our kinematical analysis to the most

recent 3.7 Gyr, which can be considered as reasonably secure. Nevertheless, we have shown that the precise shape of the temporal distributions encode a wealth of information and, therefore, more detailed analysis should be undertaken with improved observational samples. We have also extended our kinematical analysis by comparing the averaged properties of both the observational white dwarf sample and the Monte Carlo simulated sample with a sample of old main sequence F and G stars. The results of this comparison lead to the conclusion that our model of galactic evolution is fully compatible with the properties of the observed samples.

Using our synthetic populations we have assessed the completeness of the samples used to derive the white dwarf luminosity function and studied their spatial distribution, and given a set of selection criteria consistent with the observational procedures, we have built several independent realizations of the white dwarf luminosity function and compared them to the observational luminosity function of Oswalt et al. (1996). Our results regarding the white dwarf luminosity function can be summarized as follows:

(i) Given the selection criteria adopted by Oswalt et al. (1996), our Monte Carlo simulation strongly suggest that the observational samples are complete up to  $17^{\text{mag}}$  and that the primary selection criterion at low luminosities is the proper motion one, in agreement with Wood & Oswalt (1998).

(ii) The Monte Carlo simulated white dwarf luminosity functions present an excellent agreement with the observational data.

(iii) The effects of a scale height law are not negligible at all in the spatial distribution of the samples, especially at moderately large luminosities were they are more prominent. A scale height of roughly 130 pc is derived from the Monte Carlo simulations for the objects used in building the white dwarf luminosity function. However, we have established without any doubt that the effects of a scale height law should be more apparent in the cumulative distribution of proper motions. Although the effects of the scale height law on the tail of the white dwarf luminosity function seem to be negligible at first glance, a detailed analysis reveals that this inflation effect increases the derived ages of the disk by a considerable amount, which can be typically 2 Gyr.

(iv) By using Bayesian inference techniques we have been able to establish that the current procedure to assign the observational error bars to the white dwarf luminosity function is reasonable for a sample of 200 stars.

(v) Finally, the statistical uncertainty in the age of the disk derived from a Bayesian analysis is roughly 1 Gyr, in agreement with Wood & Oswalt (1998), and we have determined that there is a systematic trend due to the binning procedure which increases the disk ages inferred from the observational luminosity function by roughly a 5%.

Nevertheless, a good deal of work remains to be done. Future improvements may include a more detailed analysis of the kinematical properties of the sample of old white dwarfs. For this purpose, it would be very useful to have more reliable observational samples. In our case this means not only complete samples but also more accurate mass determinations. It would be also convenient to analyze the three dimensional motion of the white dwarf population but, for the moment, this seems to be unavoidable for the faintest white dwarfs due to the absence of spectral features. Also of

interest is to study the contamination of the input samples used in the process of building the white dwarf luminosity function with white dwarfs belonging to the galactic halo. This, in principle, cannot be discarded since halo members are selected on the basis of high proper motion, which is the dominant selection criterion at the dim end of the disk white dwarf luminosity function. A detailed statistical analysis of the cumulative counts of white dwarfs still remains to be done, instead of using the differential space density. Last but not least, the tests proposed in this paper could be applied to a real sample, thus providing us with very useful hints about the structure and evolution of our Galaxy.

*Acknowledgements* This work has been supported by DGI-CYT grants PB94-0111 and PB94-0827-C02-02, and by the CIRIT grant GRQ94-8001.

## REFERENCES

- Avni, Y., Bahcall, J.N., 1980, *ApJ*, 235, 694  
 Bergeron, P., Saffer, R.A., Liebert, J., 1992, *ApJ*, 394, 228  
 Bergeron, P., Wesemael, F., Beauchamp, A., 1995, *PASP*, 107, 1047  
 Bravo, E., Isern, J., Canal, R., 1993, *A&A*, 270, 288  
 Carney, B.W., Latham, D.W., Laird, J.B., 1990, *AJ*, 99, 572  
 Dehnen, W., Binney, J.J., 1997, *astro-ph/9710077*  
 Díaz-Pinto, A., García-Berro, E., Hernanz, M., Isern, J., Mochkovitch, R., 1994, *A&A*, 282, 86  
 Edvardsson, B., Andersen, J., Gustafsson, B., Lambert, D.L., Nissen, P.E., Tomkin, J., 1993, *A&A*, 275, 101  
 Felten, J.E., 1976, *A&AS*, 207, 700  
 Fleming, T.A., Liebert, J., Green, R.F., 1986, *ApJ*, 308, 176  
 Flynn, C., Sommer-Larsen, J., Christensen, P.R., 1996, *MNRAS*, 281, 1027  
 García-Berro, E., Hernanz, M., Mochkovitch, R., Isern, J., 1988, *A&A*, 193, 141  
 García-Berro, E., Torres, S., 1997, in *White Dwarfs*, ed. J. Isern, M. Hernanz & E. García-Berro (Kluwer Academic Publishers), 97  
 Green, R.F., 1980, *ApJ*, 238, 685  
 Hernanz, M., García-Berro, E., Isern, J., Mochkovitch, R., Segretain, L., Chabrier, G., 1994, *ApJ*, 434, 652  
 Iben, I., & Laughlin, G., 1989, *ApJ*, 341, 312  
 Isern, J., García-Berro, E., Hernanz, M., Mochkovitch, R., Burkert, A., 1995a, in *White Dwarfs*, ed. D. Koester & K. Werner (Springer Verlag), 19  
 Isern, J., García-Berro, E., Hernanz, M., Mochkovitch, R., Burkert, A., 1995b, in *The Formation of the Milky Way*, ed. E.J. Alfaro & A.J. Delgado (Cambridge University Press), 19  
 James, F., 1990, *Comput. Phys. Commun.*, 60, 329  
 Leggett, S.K., Ruiz, M.T., Bergeron, P., 1998, *ApJ*, in press  
 Liebert, J., Dahn, C.C., Monet, D.G., 1988, *ApJ*, 332, 891  
 Liebert, J., Dahn, C.C., Monet, D.G., 1989, in *White Dwarfs*, ed. G. Wegner (Springer Verlag), 15  
 Mihalas, D., Binney, J., 1981, *Galactic Astronomy* (W.H. Freeman & Co.)  
 Ng, Y.K., Bertelli, G., 1998, *A&A*, 329, 943  
 Noh, H.-R., Scalo, J., 1990, *ApJ*, 352, 605  
 Ogorodnikov, K.F., 1965, *Dynamics of Stellar Systems* (Pergamon Press)  
 Oswalt, T.D., Smith, J.A., 1995, in *White Dwarfs*, ed. D. Koester & K. Werner (Springer Verlag), 24  
 Oswalt, T.D., Smith, J.A., Wood, M.A., Hintzen, P., 1996, *Nature*, 382, 692  
 Press, W.H., 1996, in *Unsolved problems in Astrophysics* (Princeton University Press)  
 Press, W.H., Flannery, B.P., Teukolsky, S.A., Vetterling, W.T., 1986, *Numerical Recipes* (Cambridge University Press)  
 Qin, Y.P., & Xie, G.Z., 1997, *ApJ*, 486, 100  
 Salaris, M., Domínguez, I., García-Berro, E., Hernanz, M., Isern, J., Mochkovitch, R., 1997, *ApJ*, 486, 413  
 Salpeter, E.E., 1961, *ApJ*, 134, 669  
 Scalo, J., 1998, in *The Stellar Initial Mass Function*, eds. G. Gilmore, I. Parry & S. Ryan (PASP Conference Series), in press  
 Schmidt, M., 1968, *ApJ*, 151, 393  
 Sion E.M., Fritz, M.L., McMullin, J.P., Lallo, M.D., 1988, *AJ*, 96, 251  
 Sion E.M., Liebert, J., 1977, *ApJ*, 213, 468  
 Tinney, C.G., Reid, I.N., Mould, J.R., 1993, *ApJ*, 414, 254  
 Winget, D.E., Hansen, C.J., Liebert, J., Van Horn, H.M., Fontaine, G., Nather, R., Kepler, S.O., Lamb, D.K., 1987, *ApJ*, 315, L77  
 Wood, M.A., 1992, *ApJ*, 386, 539  
 Wood, M.A., 1997, in *White Dwarfs*, ed. J. Isern, M. Hernanz & E. García-Berro (Kluwer Academic Publishers), 105  
 Wood, M.A., Oswalt, T.D., 1998, *ApJ*, in press